

LETTER • OPEN ACCESS

## Both day and night warming reduce tree growth in extremely dry soils

Recent citations

- [Research challenges and opportunities for using big data in global change biology](#)  
Jianyang Xia *et al*

To cite this article: Chen Zhu *et al* 2020 *Environ. Res. Lett.* **15** 094074

View the [article online](#) for updates and enhancements.

## Environmental Research Letters



## LETTER

## OPEN ACCESS

RECEIVED  
25 July 2019

REVISED  
19 June 2020

ACCEPTED FOR PUBLICATION  
15 July 2020

PUBLISHED  
28 August 2020

Original content from  
this work may be used  
under the terms of the  
[Creative Commons  
Attribution 3.0 licence](#).

Any further distribution  
of this work must  
maintain attribution to  
the author(s) and the title  
of the work, journal  
citation and DOI.



## Both day and night warming reduce tree growth in extremely dry soils

Chen Zhu<sup>1,2</sup> , Erqian Cui<sup>1,2</sup> and Jianyang Xia<sup>1,2</sup>

<sup>1</sup> Zhejiang Tiantong Forest Ecosystem National Observation and Research Station, Shanghai Key Lab for Urban Ecological Processes and Eco-Restoration, School of Ecological and Environmental Sciences, East China Normal University, Shanghai 200241, People's Republic of China

<sup>2</sup> Center for Global Change and Ecological Forecasting, East China Normal University, Shanghai, People's Republic of China

E-mail: [jyxia@des.ecnu.edu.cn](mailto:jyxia@des.ecnu.edu.cn)

**Keywords:** asymmetric warming, biomass allocation, drought, forest growth, tree-ring

Supplementary material for this article is available [online](#)

## Abstract

Trees in global forests are exposed to warming climate, the rate of which is different between day and night, and associated with soil drought. Previous studies commonly show that forest growth responds positively to daytime warming but negatively to night warming. However, it remains unclear whether such asymmetric responses of forest growth to day and night warming still exist in extremely dry soils. Here, based on the long-term records of the normalized difference vegetation index and ring-width index at 2294 forest sites across the Northern Hemisphere, we found that the rising daytime maximum temperature ( $T_{\max}$ ) reduces stem growth but the rising nighttime minimum temperature ( $T_{\min}$ ) lowers canopy greenness when the soil is drier than a threshold. We further discuss three mechanisms that could drive such negative impacts. For example, data from experimental studies showed that the shifted biomass allocation from wood to leaves is one important mechanism driving the reductions of wood growth under day warming. These findings indicate that climate warming could negatively affect tree growth in extremely dry soils, regardless of whether temperature rises during the daytime or at night. Thus, understanding the interactions of water and temperature on the sub-diurnal scale is critical for improving our ability to predict the forest dynamics under future climate change.

## 1. Introduction

The world's forests are crucial in regulating the feedback between terrestrial ecosystems and climate change (Körner *et al* 2005, Bonan 2008, Pan *et al* 2011). In recent decades, climate has gradually become hotter and drier in many forest regions (Allen *et al* 2015). The warming climate features non-uniform temperature increases between day and night as well as spatial temperature variance (Karl *et al* 1991, Easterling *et al* 1997, Xia *et al* 2014). For example, warming is faster during the daytime than at night in forests near most regions of latitudes of 60° N (e.g. eastern Canada), but the opposite trends are widespread in other forest regions of the Northern Hemisphere (Hartman *et al* 2013, Xia *et al* 2014). The drier climate is characterized by the drying of soils over many land areas (Dai 2012), which plays a critical role in limiting terrestrial carbon uptake

(Humphrey *et al* 2018, Green *et al* 2019, Huang and Xia 2019). Thus, the sustainability of forests as a mitigator of climate change will strongly depend on how tree growth responds to day and night warming in drying soils.

Trees keep growing during both day and night, and the highest rates of wood growth occur at night (Walter *et al* 2005, Matsubara *et al* 2006, Steppe *et al* 2015). Thus, tree growth is affected by both daily maximum temperature ( $T_{\max}$ , i.e. daytime temperature) and minimum temperature ( $T_{\min}$ , i.e. nighttime temperature) (Turnbull *et al* 2002, Wilson and Luckman 2002). Asymmetric responses of terrestrial plants to day and night warming have been widely reported by studies based on manipulative experiments (Turnbull *et al* 2002, Wan *et al* 2009), long-term *in situ* monitoring (Peng *et al* 2004), space-borne measurements (Peng *et al* 2013, Xia *et al* 2014) and ecosystem modeling (Dhakhwa and Campbell

1998). These asymmetric responses, however, are mainly derived from canopy measurements, such as leaf gas exchange and the normalized difference vegetation index (NDVI). However, the majority of the standing biomass is stored in the stem rather than the canopy (Myneni et al 2001, Bloom et al 2016). Whether day and night warming still can cause asymmetric responses of tree growth in extremely dry soils remains unclear.

Many recent studies have suggested that water availability can regulate the direction of forest response to climate warming. For example, modeling analyses (Xia et al 2014, Tei et al 2017) and observations (Peng et al 2013, Tan et al 2015, Tei et al 2017) have shown increasing vegetation growth under the rising  $T_{\max}$  in northern cool and wet regions (Tan et al 2015, Tei et al 2017). However, other analyses have detected negative correlations between summer  $T_{\max}$  and tree-ring width (Lloyd and Bunn 2007, Williams et al 2010, Liu et al 2013, Vicente-Serrano et al 2013, Chen et al 2017) and NDVI (Vicente-Serrano et al 2013, Buermann et al 2014, Tan et al 2015) in dry regions in middle and high latitudes of the Northern Hemisphere. However, analyses based on empirical data, such as tree-ring records, are still scarce in exploring the different impacts of  $T_{\max}$  and  $T_{\min}$  on tree growth in extremely dry regions.

The extremely dry soils can be defined in different ways. It can be statistically quantified as time steps with soil moisture below the 10th percentile during the growing season (Nicolai-Shaw et al 2017). More ecologically, extreme dry soils damage hydraulic supply and thus inhibit tree growth with a very low soil water content (Mcdowell et al 2008, Choat et al 2018). At least three mechanisms could lead to reduced tree growth under both day and night warming in extremely dry soils. First, it is known that plants can optimize photosynthesis to adapt and/or acclimate to a rising  $T_{\max}$  (Berry and Bjorkman 1980, Yuan et al 2011, Niu et al 2012). However, the rising  $T_{\max}$  will reduce photosynthetic assimilates when it moves beyond the upper limit of the optimum temperature for gross primary productivity ( $T_{\text{opt}}^{\text{GPP}}$ ). Second, soil water availability strongly regulates vegetation growth when the temperature reaches the maximum in midday (Niu et al 2008) or in the summer (Ciais et al 2005, Williams et al 2012). Thus, drought stress would constrain tissue formations (Muller et al 2011, Körner 2013, 2015) and force a reduction in biomass allocation to wood (Way and Oren 2010, Poorter et al 2012), inhibiting stem growth under a rising  $T_{\max}$  by driving nonlinear increases in the vapor pressure deficit (figure S1 (available online at [stacks.iop.org/ERL/15/094074/mmedia](https://stacks.iop.org/ERL/15/094074/mmedia))). Third, nighttime warming would stimulate night respiration, leading to a net carbon loss on the diurnal scale. Some species of trees that grow strongest at night (Walter et al 2005, Matsubara et al 2006, Schurr et al 2006) may cease growth due to

the decreased carbohydrate content by enhanced respiration. Although night warming could trigger compensatory photosynthesis during the following day in dry ecosystems (Wan et al 2009, Peng et al 2013, Xia et al 2014), evidence is still lacking in forests to show that this process can reverse the negative effect of night warming (i.e. the stimulation of nighttime tree respiration) on canopy growth.

Here, we used the ring-width index (RWI) and NDVI data from 2294 forest sites across the Northern Hemisphere to study their correlations with the inter-annual changes in  $T_{\max}$  and  $T_{\min}$ . The RWI and NDVI data are valuable proxies for the year-to-year stem growth variability and canopy greenness, respectively. We also analyzed observations from 52 experimental studies and measurements at 31 forest eddy-flux sites to examine the three mechanisms driving the negative response of tree growth to day and night warming in extremely dry soils.

## 2. Methods

### 2.1. Tree-ring data

The International Tree Ring Data Bank (ITRDB) was established to store high-quality dendrochronological data contributed by researchers around the world. All available raw ring-width data ( $n = 7560$ ) were downloaded from the ITRDB on October 14, 2015 ([www.ncdc.noaa.gov/data-access/paleoclimatology-data/datasets/tree-ring](http://www.ncdc.noaa.gov/data-access/paleoclimatology-data/datasets/tree-ring)). Tree-ring data are direct measurements of the annual stem growth. The chronology of each site was developed from the raw ring-width following standard dendrochronological procedures (Cook and Kairiukstis 1990). The development of chronologies was achieved using the 'dplR' package (Bunn 2008). To remove the long-term growth trend, each tree-ring series was first detrended using a negative exponential curve or a linear regression line (Cook and Peters 1981). Then, the detrended tree-ring series were averaged to obtain a standard ring width chronology at each site. We selected tree-ring chronologies which contained at least 15 years of data during 1951–2013. At the same time, each chronology contains more than five samples of tree cores per year to ensure the quality of the chronology. Finally, we obtained a network of tree-ring chronologies including the following genera from 2294 sites (table S1): *Abies* ( $n = 198$ ), *Cedrus* ( $n = 32$ ), *Larix* ( $n = 198$ ), *Picea* ( $n = 422$ ), *Pinus* ( $n = 597$ ), *Pseudotsuga* ( $n = 256$ ), *Tsuga* ( $n = 162$ ), *Quercus* ( $n = 369$ ), and *Fagus* ( $n = 60$ ).

### 2.2. Satellite NDVI measurements

The NDVI is a vegetation activity index which has been widely used for quantifying vegetation greenness. There are several satellites available to obtain NDVI data. The challenge in using these satellite-based products is their relatively short time series in comparison with tree-ring records. In

this study, we used the longest time-series satellite imagery obtained from the Advanced Very High-Resolution Radiometer with a grid size of  $8 \times 8$  km during the period of 1982 to 2013 (<https://ecocast.arc.nasa.gov/data/pub/gimms/3g.v0>). The NDVI third-generation (NDVI3g) was produced by the Global Inventory Monitoring and Modeling Studies (GIMMS) group (Pinzon and Tucker 2014) and has been widely used for detecting vegetation growth trends (Piao et al 2014, Huang et al 2018). The half-monthly GIMMS-NDVI3g data were composited to monthly temporal resolution by averaging two composites in the same month. To match the resolution of climate ( $0.5^\circ$  spatial resolution), the NDVI data were resampled into  $0.5^\circ \times 0.5^\circ$  resolution. There are three main methods of resampling: nearest neighbor algorithm, bilinear interpolation and cubic convolution interpolation. Here we used the nearest neighbor algorithm to resample the NDVI data because it keeps the original value of the original image. The NDVI data used in this study were extracted from the corresponding tree-ring sites.

### 2.3. Meteorological data

Monthly meteorological data with a resolution of  $0.5^\circ \times 0.5^\circ$  including gridded  $T_{\max}$ ,  $T_{\min}$  and precipitation values were obtained from the Climate Research Unit (CRU; version 3.23; [https://crudata.uea.ac.uk/cru/data/hrg/cru\\_ts\\_3.23/](https://crudata.uea.ac.uk/cru/data/hrg/cru_ts_3.23/)) (Harris et al 2014). The solar radiation data at a  $0.5^\circ$  resolution used in our analysis were from the Terrestrial Hydrology Research Group at Princeton University (Sheffield et al 2006). This database provides near-surface meteorological data at three different resolutions for 1948–2014. We downloaded the monthly global meteorological data from the above two datasets over the period of 1951–2013. Then, the monthly  $T_{\max}$  and  $T_{\min}$  data were averaged to the growing-season (i.e. April to October (Peng et al 2013, Piao et al 2014)) mean  $T_{\max}$  and  $T_{\min}$ , respectively. The monthly precipitation and solar radiation data were summed to yield the growing-season total precipitation and solar radiation.

### 2.4. CMIP5 outputs

The simulated monthly  $T_{\max}$  from 14 Earth system models comprising the Coupled Model Intercomparison Project Phase 5 (CMIP5) (table S2) were analyzed (<https://pcmdi.llnl.gov/mips/cmip5/>). The modeled monthly  $T_{\max}$  were generated from the two representative concentration pathways (RCPs, i.e. RCP4.5 and RCP8.5) over the period of 2081 to 2100. The RCP4.5 and RCP8.5 scenarios represent the long-term global emission would stabilize radiative forcing at  $4.5 \text{ W m}^{-2}$  and  $8.5 \text{ W m}^{-2}$ , respectively (Riahi et al 2011, Thomson et al 2011). All model simulations were resampled to a  $0.5^\circ \times 0.5^\circ$  spatial resolution using nearest neighbor interpolation.

### 2.5. Soil water content data

The observation of soil moisture ( $\text{m}^3 \text{ m}^{-3}$ ) data were generated from active and passive microwave spaceborne instruments. The data covered the period of 1978–2015 with the spatial resolution of  $0.25^\circ \times 0.25^\circ$ . These data were derived from the Essential Climate Variable (ECV) Soil Moisture dataset (ECV SM 02.0) ([www.esa-soilmoisture-cci.org/](http://www.esa-soilmoisture-cci.org/)), which reflects the 0.5–2.0 cm depth layer soil water content (Liu et al 2011). We extracted the growing-season soil moisture of each year. The soil moisture dataset was not aggregated up to  $0.5^\circ$  resolution because we needed to extract values at corresponding tree-ring sites at a finer resolution.

The soil moisture can regulate the impacts of rising  $T_{\max}$  and  $T_{\min}$  values on the NDVI and RWI (figures S2(a)–(d)). To make these findings clearer, the soil moisture data were binned into increments of  $0.01 \text{ m}^3 \text{ m}^{-3}$ . The determination of the bin size followed two principles. First, the patterns of the relationships between the soil moisture and partial correlations (figures S2(a)–(d)) were not changed when the soil moisture data were binned (figures S2(e)–(h)). Second, the bin size ensured that the trend of the raw data did not change and that each bin contained enough samples (figure S3(a)). Partial correlation coefficients between the NDVI and  $T_{\max}$  ( $r_{\text{NDVI-}T_{\max}}$ ), the NDVI and  $T_{\min}$  ( $r_{\text{NDVI-}T_{\min}}$ ), the RWI and  $T_{\max}$  ( $r_{\text{RWI-}T_{\max}}$ ), and the RWI and  $T_{\min}$  ( $r_{\text{RWI-}T_{\min}}$ ) were averaged in each soil moisture bin. Linear (Hogg et al 2017, Reich et al 2018) or parabolic relationships (Joseph et al 2014) between soil moisture and tree growth have been reported in recent experimental studies, so we adopted a parabolic function when the data distribution shows a curvilinear trend. Finally, linear regression was applied to detect the correlation between the binned soil moisture and  $r_{\text{NDVI-}T_{\max}}$  and  $r_{\text{RWI-}T_{\max}}$ , while the binned soil moisture had a nonlinear relationship with  $r_{\text{NDVI-}T_{\min}}$ . No significant linear or nonlinear relationship was found between the binned soil moisture and  $r_{\text{RWI-}T_{\min}}$ .

### 2.6. Soil texture data

Since the tree-ring sites are widely distributed across the Northern Hemisphere, the soil texture would have influence on the soil water availability. The soil texture data are provided by the Harmonized World Soil Database (HWSD) for the top 30 cm of soil at a  $0.008^\circ$  resolution. The topsoil textual classes are based on the relative contents of sand, silt and clay. Sandy soil includes sand, loamy sands and sandy loams with less than 18% clay and more than 65% sand. Loamy soil includes sandy loams, loams, sandy clay loams, silt loams, silt, silty clay loams and clay loams with less than 35% clay and less than 65% sand; if the clay fraction reaches a minimum of 18%, the sand fraction may be as high as 82%. Clay soil includes clays, silty clays, sandy clays, clay loams and silty clay loams with

more than 35% clay. Here, we used the clay content data from the HWSD to indicate the soil texture.

## 2.7. Soil water potential data

The soil water potential was used as another robust indicator reflecting the water availability to plants (figures S2(e)–(h)). We ran the version 4.5 of the Community Land Model (CLM4.5) to obtain the global soil water potential data. The CLM4.5 were run retrospectively from 1951 to 2013 at a  $1^\circ \times 1^\circ$  spatial resolutions across the globe. The default meteorological forcing dataset provided with CLM4.5 is the CRUNCEP forcing dataset (<https://www.earthsystemgrid.org/dataset/ucar.cgd.cesm4.CRUNCEP.v4.TPHWL6Hrly.html>). The top two layers (0–0.7 cm and 0.7–2.8 cm) of the growing-season soil water potential were averaged and then interpolated to a  $0.5^\circ \times 0.5^\circ$  spatial resolution using nearest neighbor interpolation.

We also binned the soil water potential data following the same principles used with the soil moisture data. The bin size of the soil water potential was determined as 0.2 MPa in the range of 0 ~ 4 MPa. The values of soil water potentials larger than 5 MPa were binned into one group because the number of soil water potentials larger than 5 MPa is relatively small (figure S3). The  $r_{NDVI-T_{max}}$ ,  $r_{NDVI-T_{min}}$ ,  $r_{RWI-T_{max}}$  and  $r_{RWI-T_{min}}$  were averaged in each soil water potential bin.

## 2.8. Carbon fluxes dataset

The calculation of  $T_{opt}^{GPP}$  was based on measurements of GPP at 31 forest flux sites across the Northern Hemisphere. The geographical distributions of the flux sites are shown in figure S4. The data are available in the FLUXNET 2015 dataset at [www.fluxcom.org/](http://www.fluxcom.org/). The raw carbon dioxide records have been harmonized, standardized and gap-filled (Papale *et al* 2006). In total, 31 forest sites with >5 years of observations were selected for further calculation of the  $T_{opt}^{GPP}$  (table S3). We used the daily temperature and GPP rather than hourly or monthly values to characterize the phenological changes over a growing season. As shown by Niu *et al* (2012), based on a  $1^\circ\text{C}$  temperature bin, the daily temperature and GPP for each site and year were averaged in each temperature bin. The running mean of every three temperature bins was calculated, and the temperature at which GPP is maximized was obtained as the  $T_{opt}^{GPP}$  at each site (figure S5). The mean  $T_{opt}^{GPP}$  across the 31 forest sites was  $21.2 \pm 4.0^\circ\text{C}$ .

## 2.9. Biomass allocation data

Observations of the biomass allocation in trees under experimental warming and drought conditions were collected from published literature. There were a total of 52 experiments which reported the biomass

responses of leaves, wood and fine roots to experimental warming or drought. The studies are listed in the supporting information (supplementary section 2). Due to the lack of field experiments in forests, it should be noted that the observations were mainly obtained from saplings or seedlings in greenhouse experiments. Therefore, cautions should be taken in extrapolating experimental findings on seedlings to adult trees. The carbon allocations in seedling trees are expected to respond earlier to low temperature and drought stress than adult trees (Hartmann *et al* 2018). This is because growth would reduce before photosynthesis, while seedling trees have smaller pools of water and non-structural carbohydrates to be depleted.

Although a mass of experiments has been carried out to study the response of biomass allocation to temperature and drought stress, the experimental settings and plant species vary among different experiments. Thus, a method to generalize data from a wide range of experiments would enable quantitative and comparative analyses. To quantify the response of tree biomass allocation to temperature change and drought stress, we referred to the approach of dose-response curves developed by Poorter *et al* (2010). This methodology enables us to generalize responses from various experiments and species in a continuous manner. Moreover, such response curves enable quantification of the strength, sign and form of a given factor's impact on biomass allocation over the full relevant range of that factor. It has been successfully used for quantifying the investment of plant traits under the effects of 12 abiotic factors (Poorter *et al* 2012). Here, we take the response-curve of the wood biomass allocation to temperature as an example. In our database, various warming levels were applied to different conditions and species (figure S6(a)). The temperature-response curve of biomass allocation cannot be directly established from such a database. Thus, it is necessary to generalize the various experimental data by scaling both temperature and biomass allocation data. We found that the temperature in the different experiments ranged from  $8.0^\circ\text{C}$  to  $33.3^\circ\text{C}$  and most covered  $18.0^\circ\text{C}$ . Thus,  $18.0^\circ\text{C}$  was chosen as the reference temperature to scale the results from different studies. For example, the scaled value of wood biomass from different experiments was calculated by subtracting its value at a temperature of  $18.0^\circ\text{C}$  (figure S6(b)). If a temperature of  $18.0^\circ\text{C}$  was out of range (e.g. Experiment C in figure S6(a)), these data were excluded from further analysis (figure S6(b)). Following the above methods, all wood biomass for each experiment and temperature level relative to the wood biomass observed at a temperature of  $18.0^\circ\text{C}$  were calculated (figure S6(c)). Finally, the response curve was constructed by performing a piecewise regression between the temperature and the normalized wood biomass (figure S6(d)). The piecewise



regressions were applied with two, three or four linear segments using OriginPro 2016 software (Origin-Lab Corp., Northampton, MA, U.S.A.). The number of segments used to select the model was determined by testing the significance. Segment breakpoints were determined by the software during optimization. Note that the last step is different from Poorter *et al* (2010), because the small sample size of biomass allocation data in our study cannot be used for calculating the median response. There are some differences between the construction of drought-response curve (figure 4(b)) and temperature-response curve (figure 4(a)). Since drought stress (i.e. reduction in water availability) is a relative unit rather than an absolute value, we did not scale the drought stress (on the  $x$ -axis). The woody biomass allocation (on the  $y$ -axis) was scaled by the reduction in plant biomass relative to the control group with each experiment. The drought-response curves of biomass allocation were also constructed by performing a piecewise regression between the reduction in water availability and the scaled wood biomass.

## 2.10. Uncertainty assessment

Due to the small sample size of the biomass allocation data, a bootstrapping method was used to estimate the uncertainties of segment breaks in figure 4. We constructed a resampled dataset with the same size as the observed dataset by sampling with replacement from the original data. Then the breakpoint was estimated from each resampled dataset. Repeating this process, we obtained 1000 breakpoints from 1000 bootstrap samples. The uncertainties of segment breaks were shown by computing a mean and standard deviation.

## 2.11. Statistical analyses

Tree growth has been attributed to interactions between environmental variables, such as temperature, precipitation and solar radiation (Vaganov *et al* 2006, Babst 2019). Thus, the covariance of precipitation and solar radiation needs to be considered in the analysis of the correlations between the NDVI or RWI and diurnal temperatures. Here, we applied partial correlation analysis to examine the correlations between the RWI or NDVI and the  $T_{\max}$  or  $T_{\min}$  by removing the confounding effects of precipitation and solar radiation. The partial correlation can be explained as the correlation between random variables after eliminating the effect of all other random variables. Mathematically, the definition of partial correlation can be described as:

$$r_{12,3} = (r_{12} - r_{13} \times r_{23}) / \sqrt{(1 - r_{13}^2)(1 - r_{23}^2)} \quad (1)$$

where  $r_{12}$  is the correlation between  $x_1$  and  $x_2$ ,  $r_{13}$  is the correlation between  $x_1$  and  $x_3$ ,  $r_{23}$  is the correlation between  $x_2$  and  $x_3$ . This equation can be further extended to the higher-order partial correlations.

For this purpose, we need to use the inverse variance-covariance matrix of  $\mathbf{X}$ :

$$\mathbf{D}_\mathbf{X} = \mathbf{C}_\mathbf{X}^{-1} \quad (2)$$

Here, we define  $\mathbf{D}_\mathbf{X}$  as  $(d_{ij})$  and  $\mathbf{C}_\mathbf{X}$  as  $(c_{ij})$ , where  $d_{ij}$  and  $c_{ij}$  are the  $(i,j)$ -th cell of matrices  $\mathbf{D}_\mathbf{X}$  and  $\mathbf{C}_\mathbf{X}$ . The partial correlation of  $x_i$  and  $x_j$  given a random vector  $\mathbf{X}_S$  can be described as:

$$r_{ij,S} = -d_{ij} / \sqrt{d_{ii}} \sqrt{d_{jj}} \quad (3)$$

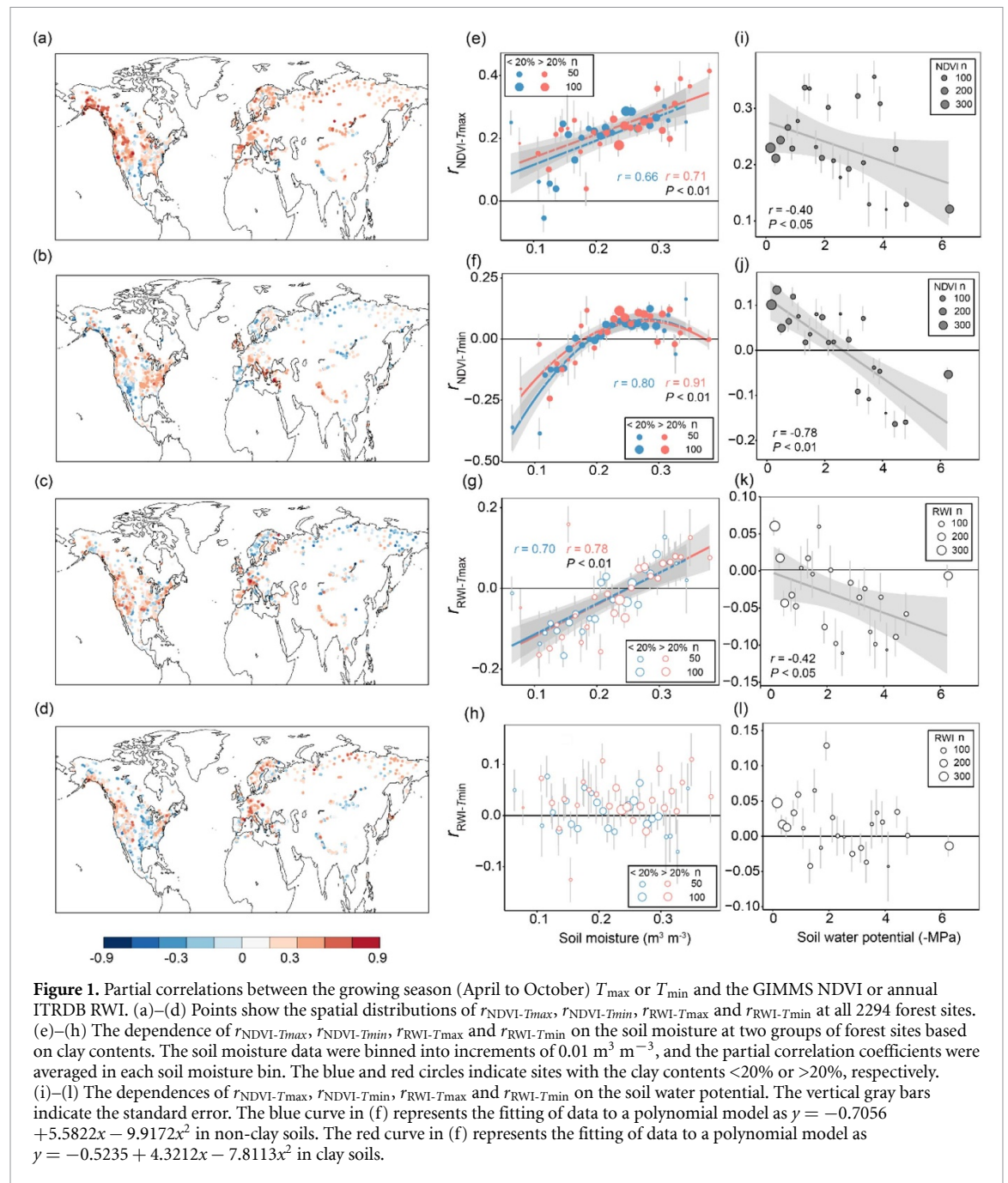
The method has been widely used to measure the correlations between vegetation growth and a given environmental factor by controlling the confounding effects of other variables (Peng *et al* 2013, Xia *et al* 2014). More specifically, when analyzing the relationship between the RWI/NDVI and the  $T_{\max}$  (i.e.  $r_{\text{RWI-}T_{\max}}$  and  $r_{\text{NDVI-}T_{\max}}$ ), we considered the  $T_{\min}$ , precipitation and solar radiation as the confounding variables. Similarly, for analyzing the partial correlation between the RWI/NDVI and the  $T_{\min}$  (i.e.  $r_{\text{RWI-}T_{\min}}$  and  $r_{\text{NDVI-}T_{\min}}$ ), the effects of the  $T_{\max}$ , precipitation and solar radiation were considered as the confounding variables. All of the partial correlation analyses were conducted with the 'ppcor' package in R ([www.R-project.org/](http://www.R-project.org/)). The R codes for the partial correlation analysis are attached in the supplementary material file (supplementary section 1). The estimated partial correlation coefficients (i.e.  $r_{\text{RWI-}T_{\max}}$ ,  $r_{\text{NDVI-}T_{\max}}$ ,  $r_{\text{NDVI-}T_{\min}}$  and  $r_{\text{RWI-}T_{\min}}$ ) were used as the contributions of diurnal warming to the changes in canopy greenness and stem growth.

## 3. Results

### 3.1. Relationships of $T_{\max}$ and $T_{\min}$ to NDVI and RWI

By removing the confounding factors, we detected positive partial correlation coefficients between inter-annual changes in the NDVI and  $T_{\max}$  ( $r_{\text{NDVI-}T_{\max}}$ ) from 1982 to 2013 at >80% of the 2294 sites, with an average of  $0.22 \pm 0.24$  (mean  $\pm$  SD) (figure 1(a)). On the contrary, the effects of rising  $T_{\min}$  on NDVI/RWI and the effects of rising  $T_{\max}$  on RWI show large spatial variations across the Northern Hemisphere. The partial correlation coefficients between the NDVI and  $T_{\min}$  ( $r_{\text{NDVI-}T_{\min}}$ ) were positive at approximately 55% of all sites, and the average  $r_{\text{NDVI-}T_{\min}}$  was  $0.03 \pm 0.24$  (figure 1(b)). The mean values of partial correlation coefficients between the RWI and  $T_{\max}$  ( $r_{\text{RWI-}T_{\max}}$ ) and the RWI and  $T_{\min}$  ( $r_{\text{RWI-}T_{\min}}$ ) from 1951–2013 were  $-0.02 \pm 0.24$  and  $0.02 \pm 0.22$ , respectively (figures 1(c) and (d)).

All 2294 sites were separated into two groups based on clay contents of <20% (non-clay soils) and >20% (clay soils). Both  $r_{\text{NDVI-}T_{\max}}$  and  $r_{\text{RWI-}T_{\max}}$  depended positively and linearly on the soil moisture in both non-clay and clay soils (all  $P < 0.01$ , figures



1(e) and (g)). The average values of  $r_{\text{NDVI-}T_{\max}}$  over most soil moisture bins were positive (figure 1(e)), whereas there was a transition of the  $r_{\text{RWI-}T_{\max}}$  from negative to positive at a soil moisture of  $0.25 \text{ m}^3 \text{ m}^{-3}$  in both non-clay and clay soils (figure 1(g)). Soil moisture had a nonlinear relationship with  $r_{\text{NDVI-}T_{\min}}$  in both non-clay ( $r = 0.80$ ,  $P < 0.01$ ; figure 1(f)) and clay soils ( $r = 0.91$ ,  $P < 0.01$ ; figure 1(f)). No significant relationship between the soil moisture and  $r_{\text{RWI-}T_{\min}}$  was found across all sites (figure 1(h)).

Given that the major limitation of soil moisture data is its reliance on soil texture, we also examined the influences of the soil water potential on the partial correlation coefficients between NDVI/RWI and  $T_{\max}/T_{\min}$ . Soil water potential had negative and linear relationships with  $r_{\text{NDVI-}T_{\max}}$

( $r = -0.40$ ,  $P < 0.05$ ; figure 1(i)),  $r_{\text{NDVI-}T_{\min}}$  ( $r = -0.78$ ,  $P < 0.01$ ; figures 1(j)) and  $r_{\text{RWI-}T_{\max}}$  ( $r = -0.42$ ,  $P < 0.05$ ; figure 1(k)) but had no significant impact on  $r_{\text{RWI-}T_{\min}}$  (figure 1(l)). The transitions of  $r_{\text{NDVI-}T_{\min}}$  and  $r_{\text{RWI-}T_{\max}}$  from positive to negative values occurred at the soil water potentials of approximately 2.54 MPa and 0.15 MPa, respectively (figures 1(j) and (k)).

The spatial distribution of the gridded forest regions that may be negatively affected by day or night warming during 1979–2013 across the Northern Hemisphere were mapped based on the soil moisture threshold found in figures 1(f) and (g). The effects of rising  $T_{\max}$  and  $T_{\min}$  on forest growth were both negative in some regions such as western America and southern Siberia (figure 2).

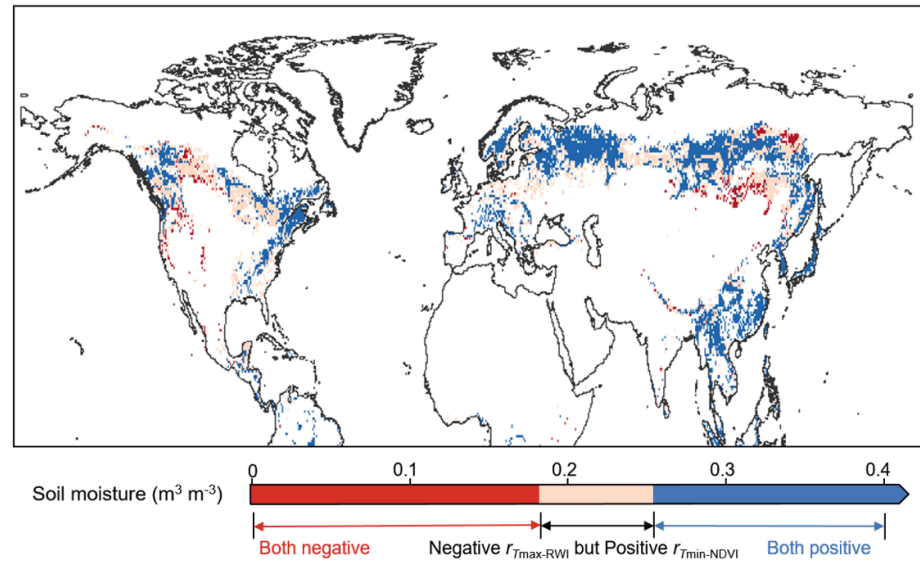


**Figure 2.** Spatial distribution of the gridded forest regions that may be negatively affected by rising  $T_{\max}$  or  $T_{\min}$  across the Northern Hemisphere at the  $0.5^\circ$  resolution. The ECV soil moisture data during growing season between 1979 and 2013 were used to map the location of the forests negatively affected by rising  $T_{\max}$  or  $T_{\min}$ . The red regions indicate that soil moisture is less than  $0.18 \text{ m}^3 \text{ m}^{-3}$  in clay soils and  $0.19 \text{ m}^3 \text{ m}^{-3}$  in non-clay soils, where the NDVI is negatively affected by rising  $T_{\min}$  and RWI is negatively affected by rising  $T_{\max}$ . The pink regions indicate that soil moisture is less than  $0.25 \text{ m}^3 \text{ m}^{-3}$ , where the rising  $T_{\max}$  negatively affect RWI but  $T_{\min}$  positively affect NDVI. The blue regions indicate that soil moisture is greater than  $0.25 \text{ m}^3 \text{ m}^{-3}$ , where both NDVI and RWI are positively affected by rising  $T_{\max}$  and  $T_{\min}$ . The classification of vegetation types was based on MODIS land cover product MCD12C1 (Fredlund and Xing 1994, Friedl et al 2010).

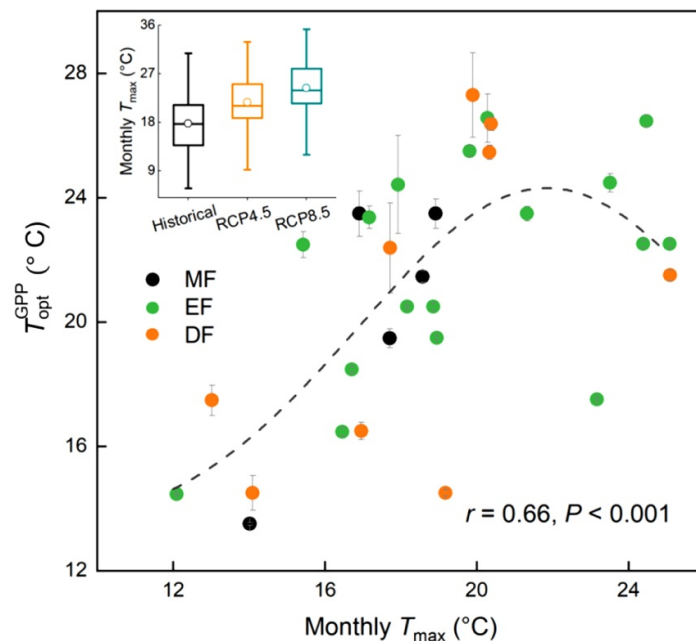


**Figure 3.** Saturation of the  $T_{\text{opt}}^{\text{GPP}}$  to the rising  $T_{\max}$  across the eddy-flux sites. Due to the temperature response of photosynthesis can be described with a peak curve, a Gaussian regression model is used to fit the data ( $T_{\text{opt}}^{\text{GPP}} = 13.11 + 11.2 \times e^{-0.5 \times \left( \frac{T_{\max} - 21.85}{4.92} \right)^2}$ ) ( $R^2 = 0.66$ ,  $P < 0.001$ ). The 31 eddy-flux sites were grouped into three categories based on the plant functional type (MF: mixed forest, EF: evergreen forest and DF: deciduous forest). The inset shows the monthly  $T_{\max}$  during 1951–2013 based on the CRU3.23 dataset and during 2081–2100 from the CMIP5 models under the RCP4.5 and RCP8.5 scenarios. Boxes indicate the 25% and 75% quartiles, whiskers indicate the extent of the data, lines indicate the median, and circles indicate the mean.

### 3.2. Dependence of $T_{\text{opt}}^{\text{GPP}}$ on $T_{\max}$

The measured daily GPP generally changed nonlinearly with temperature at all 31 eddy-flux sites in this study (figure S5). Since the nonlinear relationships

all follow the peak curve, the  $T_{\text{opt}}^{\text{GPP}}$  was calculated as the peak value of the curve at each site. Spatially, the  $T_{\text{opt}}^{\text{GPP}}$  nonlinearly increased with the monthly  $T_{\max}$  ( $r = 0.66$ ,  $P < 0.001$ ; figure 3).



We then compared the historical and future projected monthly  $T_{\max}$  values across the 2294 forest sites with the averaged  $T_{\text{opt}}^{\text{GPP}}$  value from the eddy-flux sites (i.e.  $21.2 \pm 4.0$  °C). We found that the historical monthly  $T_{\max}$  between 1951 and 2013 ( $17.8 \pm 5.1$  °C) was significantly lower than the estimate from the eddy-flux sites ( $P < 0.05$ ; figure 3 inset). However, the future monthly  $T_{\max}$  between 2081 and 2100 under both the RCP4.5 ( $21.7 \pm 4.9$  °C) and RCP8.5 ( $24.3 \pm 4.9$  °C) scenarios were significantly higher than the estimate from the eddy-flux sites (both  $P < 0.05$ ; figure 3 inset).

### 3.3. Tree biomass allocation under experimental warming and drought

Observations from 8 warming experiments and 44 drought experiments across the Northern Hemisphere were collected to examine the effects of warming and drought on the biomass allocation of trees (figure S7). The piecewise regression analysis showed that trees allocated more biomass to leaves when the temperature was higher than 28.0 °C ( $r^2 = 0.37$ ,  $P < 0.05$ ; the average bootstrapped breakpoint was  $26.5 \pm 3.1$ ) but less to the wood when the temperature was  $>25.1$  °C ( $r^2 = 0.31$ ,  $P < 0.05$ ; the average bootstrapped breakpoint was  $25.5 \pm 2.7$ ; figure 4(a)). In the drought experiments, trees also significantly reduced their allocations to stem growth when the soil water availability was reduced by more than 70% ( $r^2 = 0.40$ ,  $P < 0.05$ ; the average bootstrapped breakpoint was  $0.39 \pm 0.09$ ; figure 4(b)). However, leaf allocation was not significantly affected by the 50% reduction in soil water availability in these experiments ( $r^2 = 0.02$ ,  $P = 0.12$ ; the average bootstrapped breakpoint was  $0.43 \pm 0.16$ ; figure 4(b)).

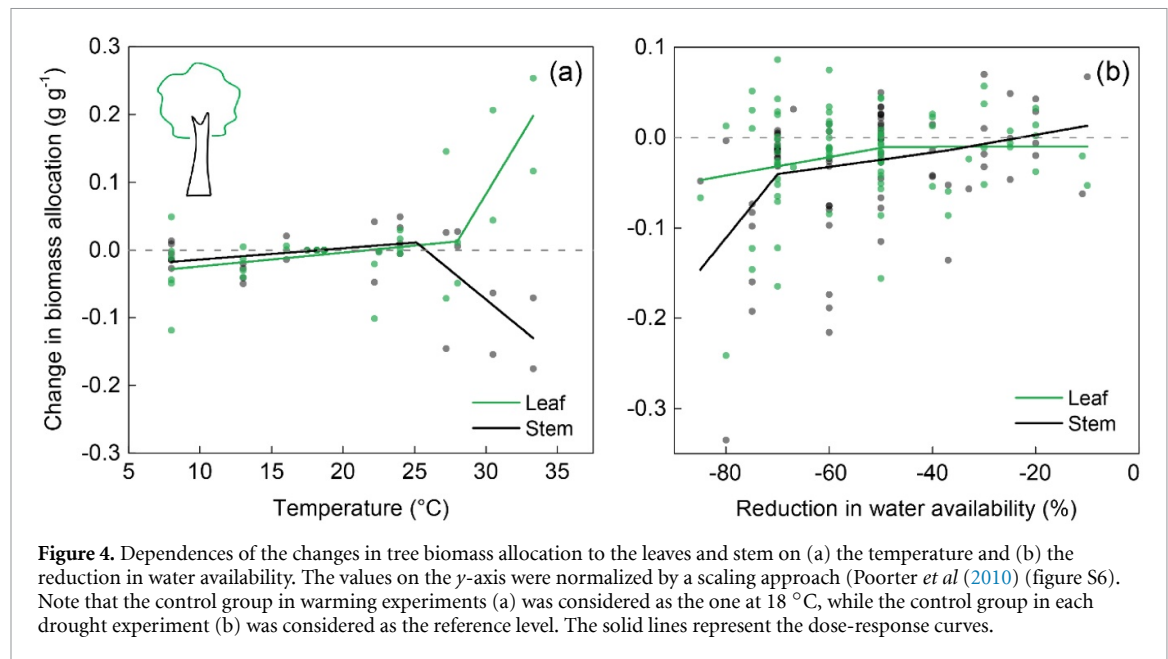
## 4. Discussion

Based on different vegetation indices, this study found that day warming negatively affects stem growth, while night warming decreases canopy greenness in extremely dry regions (figures 1(f), (g), (j) and (k)). Such negative responses of tree growth to both day and night warming are not well-captured by current global land surface models, which commonly predict positive impacts of a rising  $T_{\max}$  on vegetation growth in forest regions (Xia et al 2014, Tan et al 2015, Tei et al 2017). A rising  $T_{\max}$  positively affects the NDVI across the forest sites (figure 1(a)), partially because the historical  $T_{\max}$  is still lower than the  $T_{\text{opt}}^{\text{GPP}}$  (figure 3 inset). Interestingly, we found that the  $T_{\text{opt}}^{\text{GPP}}$  has an upper limit of approximately 24.3 °C (figure 3). This value is higher than the averaged  $T_{\max}$  across all the sites under the RCP4.5 but not the RCP8.5 scenario at the end of this century (figure 3 inset). This finding raises a hypothesis of a saturated optimum temperature for

canopy photosynthesis (or ' $T_{\text{opt}}^{\text{GPP}}$  saturation hypothesis') in forest ecosystems under day warming. In extremely dry regions, this study shows that the positive impacts of the rising  $T_{\max}$  on NDVI decrease rapidly ( $k_{\text{non-clay soils}} = 0.77$ ,  $k_{\text{clay soils}} = 0.73$ ; figure 1(e)). This pattern could partially result from that the enhanced tree biomass allocation to leaves under high temperature is dampened by drought (figure 4).

The reduced stem allocation under rising  $T_{\max}$  values and the associated drought (figure 4) could be an important mechanism driving the negative partial correlation coefficients between the  $T_{\max}$  and RWI in extremely dry soils (figure 1(g)). Some previous meta-analyses (Way and Oren 2010, Poorter et al 2012) have indicated that terrestrial plants would allocate more biomass to leaves than to stems under extremely hot and dry conditions. In addition, one important implication of this finding is that the response of tree growth to a rising  $T_{\max}$  cannot be simply inferred from the canopy growth. Thus, the positive correlations between the  $T_{\max}$  and satellite-derived vegetation indices reported by previous studies (Peng et al 2013, Xia et al 2014, Tan et al 2015) do not necessarily suggest an enhanced tree growth under day warming. On the other hand, experimental studies have found that drought would lead to an accumulation of non-structural carbohydrates especially soluble sugars in woody plants (Bogeat-Triboulot et al 2007, Du et al 2020). Such an increase in non-structural carbohydrates was due to growth being affected earlier and more intensively than photosynthesis (Mkr et al 2004, Muller et al 2011, Körner 2013, 2015). Therefore, stem growth may not be controlled by photosynthesis under water shortage.

Tree growth continues at night by consuming starch accumulated in the light (Schurr et al 2006, Du et al 2020). Experimental evidence has suggested that nighttime warming can negatively affect canopy growth by directly stimulating autotrophic respiration (Turnbull et al 2004) and hence to decreased carbohydrate content used to support growth. At the same time, the combined water shortage can decrease chlorophyll content (Eastman and Camm 1995, Ogaya et al 2011) and reduce stomatal conductance (Jing et al 2016). However, some previous studies have hypothesized a phenomenon of 'photosynthetic overcompensation' under night warming (Turnbull et al 2002, Wan et al 2009, Xia et al 2014), which shows that the 'source' activity (that is, photosynthesis) will be enhanced when depletion of the 'sink' (that is, carbohydrate storage) is increased by warmer nights (Körner 2003). In tree species, the existence of photosynthetic overcompensation effect under night warming has been either observed (Turnbull et al 2002) or undetected (Bruhn et al 2007, Ibrahim et al 2010) in seedling experiments. Quantifying the contribution of this effect to the nonlinear pattern in figure 1(f) is impossible using currently available data sets. However, as shown by figure 1(f),



the strength of ‘photosynthetic overcompensation’ in tree species under night warming would diminish under soil drying.

It should be noted that there are several limitations in this study. First, the scale mismatch for the comparison of tree-ring data and satellite NDVI data adds uncertainty in the analyses. The inconsistent response of RWI and NDVI to diurnal warming could be the vegetation change in forests (Tei *et al* 2019) or the differences between different response from different vegetation types (Teuling *et al* 2010, Vicente-Serrano *et al* 2013). Second, most sample sites in the ITRDB are from the cold or dry edge of a species’ distribution, which have overestimated the impacts of climate change on tree growth in the US Southwest (Klesse *et al* 2018b). Although such overestimation has not been found in Central and Northern Europe (Klesse *et al* 2018a), it needs to carefully treat the climate-tree growth relationships obtained from ITRDB tree-ring records (Babst *et al* 2018). Indeed, direct eddy-flux observations would be more precise to study the day and night warming effects on vegetation productivity for they can provide diurnal scale measurements. However, daily measurements would more reflect the impacts of  $T_{\max}$  and  $T_{\min}$  on the seasonal changes of productivity (see supplementary text 1.2). Moreover, when daily values were aggregated to growing-season values, only a few sites captured the significant impact of day and night warming on productivity (see supplementary text 1.3). These results call for more efforts in collecting long-term eddy-flux tower data, because the observation periods of most sites in current FLUXNET datasets are not long enough for us to apply the analyses. Third, some confounding environmental factors have not been considered in our analyses, such as previous-autumn to current-spring temperature (Tei *et al* 2017) and fire

(Santoro *et al* 2001). Furthermore, it should be noted that soil moisture data used in study only represent the surface soil (0.5 to 2 cm depth). Some conifer tree species can extract water from the depth of 40–50 cm (Grossiord *et al* 2014), so it remains unclear how the vertical dynamics in soil moisture affect the results in this study. A small proportion of tree-ring sites (totally 95 out 2294 sites) were located in subtropical and tropical regions (i.e. latitudes lower than 30°N). Thus, the definition of growing season (i.e. April to October) may not appropriate for these sites due to their unclear seasonality in vegetation dynamics, which adds some uncertainty to the results. Lastly, RWI and NDVI are not measurements of biomass accumulation. Thus, analyzing the response of tree growth to diurnal warming without considering pervasive drought legacies (Anderegg *et al* 2015) and disturbances, such as logging, harvest (Amiro *et al* 2010) and fire (Hicke *et al* 2012), or mortality (Gaylord *et al* 2013, Allen *et al* 2015) is insufficient to extrapolate the carbon sink of forest.

In summary, this study suggests that both day and night warming can trigger negative impacts on tree growth when the soil is extremely dry. This finding is inconsistent with the reported asymmetric response of vegetation growth to day and night warming on the global scale (Peng *et al* 2013, Xia *et al* 2014). In fact, some recent regional and global tree-ring based analyses have suggested that the tree growth in dry regions becomes more limited by moisture as a result of climate warming (Babst 2019, Schurman *et al* 2019). It should be noted that forest growth in extremely dry regions can also be affected by other global-change factors, such as elevated CO<sub>2</sub> concentrations (Long *et al* 2004, Ainsworth and Long 2005, Ciais *et al* 2014), insect outbreaks (Breshears *et al* 2005) and fires (van Mantgem *et al* 2013). Overall,

this study calls for more experimental studies to explore the underlying mechanism of water-mediated warming effects on tree growth at the sub-diurnal scale.

## Acknowledgments


We thank the five anonymous reviewers for their constructive comments and suggestions. We also wish to thank Kun Huang for the data processing assistance, Jing Wang for her comments on mapping the results, Chenyu Bian, Zhao Li, Heming Liu and Xiaoying Sun for the code assistance. This study was supported by the National Natural Science Foundation (31722009) and the Fok Ying-Tong Education Foundation for Young Teachers in the Higher Education Institutions of China (Grant 161016), and the National 1000 Young Talents Program of China. All tree-ring data are available at International Tree Ring Data Bank. We thank all data contributors who share tree-ring data publicly. The model simulations analyzed in this study were obtained from the Earth System Grid Federation CMIP5 online portal hosted by the Program for Climate Model Diagnosis and Intercomparison at Lawrence Livermore National Laboratory (<https://pcmdi.llnl.gov/mips/cmip5/>). This work used eddy covariance data acquired and shared by the FLUXNET community, including these networks: AmeriFlux, AfriFlux, AsiaFlux, CarboAfrica, CarboEuropeIP, CarboItaly, CarboMont, ChinaFlux, Fluxnet-Canada, GreenGrass, ICOS, KoFlux, LBA, NECC, OzFlux-TERN, TCOS-Siberia, and USCCC. The ERA-Interim reanalysis data are provided by ECMWF and processed by LSCE. The FLUXNET eddy covariance data processing and harmonization was carried out by the European Fluxes Database Cluster, AmeriFlux Management Project, and Fluxdata project of FLUXNET, with the support of CDIAC and ICOS Ecosystem Thematic Center, and the OzFlux, ChinaFlux and AsiaFlux offices.

## Data availability

Any data that support the findings of this study are included within the article and its Supplementary Information files. The data that support the findings of this study are openly available at [www.ncdc.noaa.gov/data-access/paleoclimatology-data/datasets/tree-ring](http://www.ncdc.noaa.gov/data-access/paleoclimatology-data/datasets/tree-ring), <https://ecocast.arc.nasa.gov/data/pub/gimms/3g.v0>, doi:10.1002/joc.3711, [www.esa-soilmoisture-cci.org/](http://www.esa-soilmoisture-cci.org/), <https://pcmdi.llnl.gov/mips/cmip5/>, <https://doi.org/10.1016/j.rse.2017.07.001>, [www.fao.org/soils-portal/soil-survey/soil-maps-and-databases/harmonized-world-soil-database-v12/en/](http://www.fao.org/soils-portal/soil-survey/soil-maps-and-databases/harmonized-world-soil-database-v12/en/), and [www.fluxdata.org](http://www.fluxdata.org).

## ORCID iDs

Chen Zhu  <https://orcid.org/0000-0002-4104-8591>

Erqian Cui  <https://orcid.org/0000-0002-2639-5069>

Jianyang Xia  <https://orcid.org/0000-0001-5923-6665>

## References

- Ainsworth E A and Long S P 2005 What have we learned from 15 years of free-air CO<sub>2</sub> enrichment (FACE)? A meta-analytic review of the responses of photosynthesis, canopy properties and plant production to rising CO<sub>2</sub> *New Phytol.* **165** 351–71
- Allen C D, Breshears D D and McDowell N G 2015 On underestimation of global vulnerability to tree mortality and forest die-off from hotter drought in the Anthropocene *Ecosphere* **6** art129
- Amiro B D *et al* 2010 Ecosystem carbon dioxide fluxes after disturbance in forests of North America *J. Geophys. Res. Biogeosci.* **115** 4869–90
- Anderegg W R *et al* 2015 Pervasive drought legacies in forest ecosystems and their implications for carbon cycle models *Science* **349** 528–32
- Babst F 2019 Twentieth century redistribution in climatic drivers of global tree growth *Sci. Adv.* **5** eaat4313
- Babst F *et al* 2018 When tree rings go global: challenges and opportunities for retro- and prospective insight *Quat. Sci. Rev.* **197** 1–20
- Berry J and Bjorkman O 1980 Photosynthetic response and adaptation to temperature in higher plants *Annu. Rev. Plant Physiol.* **31** 491–543
- Bloom A A, Exbrayat J F, van der Velde I R, Feng L and Williams M 2016 The decadal state of the terrestrial carbon cycle: global retrievals of terrestrial carbon allocation, pools, and residence times *Proc. Natl Acad. Sci. USA* **113** 1285–90
- Bogeat-Triboulot M B *et al* 2007 Gradual soil water depletion results in reversible changes of gene expression, protein profiles, ecophysiology, and growth performance in *Populus euphratica*, a poplar growing in arid regions *Plant Physiol.* **143** 876–92
- Bonan G B 2008 Forests and climate change: forcings, feedbacks, and the climate benefits of forests *Science* **320** 1444–9
- Breshears D D *et al* 2005 Regional vegetation die-off in response to global-change-type drought *Proc. Natl. Acad. Sci. USA* **102** 15144–8
- Bruhn D A N, Egerton J J G, Loveys B R and Ball M C 2007 Evergreen leaf respiration acclimates to long-term nocturnal warming under field conditions *Glob. Change Biol.* **13** 1216–23
- Buermann W, Parida B, Jung M, Macdonald G M, Tucker C J and Reichstein M 2014 Recent shift in Eurasian boreal forest greening response may be associated with warmer and drier summers *Geophys. Res. Lett.* **41** 1995–2002
- Bunn A G 2008 A dendrochronology program library in R (dplR) *Dendrochronologia* **26** 115–24
- Chen L, Huang J G, Alam S A, Zhai L, Dawson A, Stadt K J and Comeau P G 2017 Drought causes reduced growth of trembling aspen in western Canada *Glob. Change Biol.* **23** 2887–902
- Choat B, Brodribb T J, Brodersen C R, Duursma R A, Lopez R and Medlyn B E 2018 Triggers of tree mortality under drought *Nature* **558** 531–9
- Ciais P *et al* 2005 Europe-wide reduction in primary productivity caused by the heat and drought in 2003 *Nature* **437** 529–33
- Ciais P, Sabine C, Bala G, Bopp L, Brovkin V, Canadell J, Chhabra A, Defries R, Galloway J and Heimann M 2014 Carbon and other biogeochemical cycles *Climate Change 2013: The*

- Physical Science Basis Contribution of Working Group I to the Fifth Assessment Report of the Intergovernmental Panel on Climate Change* (Cambridge: Cambridge University Press) pp 465–570
- Cook E R and Kairiukstis L A 1990 *Methods of Dendrochronology: Applications in the Environmental Sciences* (Dordrecht: Springer)
- Cook E R and Peters K 1981 The smoothing spline: a new approach to standardizing forest interior tree-ring width series for dendroclimatic studies *Tree-Ring Bull.* **41** 45–53
- Dai A 2012 Increasing drought under global warming in observations and models *Nat. Clim. Change* **3** 52–58
- Dhakhwa G B and Campbell C L 1998 Potential effects of differential day-night warming in global climate change on crop production *Clim. Change* **40** 647–67
- Du Y, Lu R, Xia J and Martin A 2020 Impacts of global environmental change drivers on non-structural carbohydrates in terrestrial plants *Funct. Ecol.* **00** 1–12
- Easterling D R *et al* 1997 Maximum and minimum temperature trends for the globe *Science* **277** 364–7
- Eastman P A K and Camm E L 1995 Regulation of photosynthesis in interior spruce during water stress: changes in gas exchange and chlorophyll fluorescence *Tree Physiol.* **15** 229–35
- Fredlund D G and Xing A 1994 Equations for the soil–water characteristic curve *Can. Geotech. J.* **31** 521–32
- Friedl M A, Sulla-Menashe D, Tan B, Schneider A, Ramankutty N, Sibley A and Huang X 2010 MODIS Collection 5 global land cover: algorithm refinements and characterization of new datasets *Remote Sens. Environ.* **114** 168–82
- Gaylord M L, Kolb T E, Pockman W T, Plaut J A, Yopez E A, Macalady A K, Pangle R E and McDowell N G 2013 Drought predisposes pinon-juniper woodlands to insect attacks and mortality *New Phytol.* **198** 567–78
- Green J K, Seneviratne S I, Berg A M, Findell K L, Hagemann S, Lawrence D M and Gentile P 2019 Large influence of soil moisture on long-term terrestrial carbon uptake *Nature* **565** 476–9
- Grossiord C, Gessler A, Granier A, Berger S, Bréchet C, Hentschel R, Hommel R, Scherer-Lorenzen M and Bonal D 2014 Impact of interspecific interactions on the soil water uptake depth in a young temperate mixed species plantation *J. Hydrol.* **519** 3511–9
- Harris I, Jones P D, Osborn T J and Lister D H 2014 Updated high-resolution grids of monthly climatic observations - the CRU TS3.10 Dataset *Int. J. Climatol.* **34** 623–42
- Hartman D L, Tank A M G K, Rusicucci M, Alexander L V, Broenniman B, Charabi Y, Dentener F J, Dlugokencky E J, Easterling E R and Kaplan A 2013 Observations: atmosphere and surface *Climate Change 2013: The Physical Science Basis. Contribution of Working Group I to the Fifth Assessment Report of the Intergovernmental Panel on Climate Change* ed T F Stocker *et al* (Cambridge and New York: Cambridge University Press) pp 159–254
- Hartmann H, Adams H D, Hammond W M, Hoch G, Landhäusser S M, Wiley E and Zaehle S 2018 Identifying differences in carbohydrate dynamics of seedlings and mature trees to improve carbon allocation in models for trees and forests *Environ. Exp. Bot.* **152** 7–18
- Hicke J A *et al* 2012 Effects of biotic disturbances on forest carbon cycling in the United States and Canada *Glob. Change Biol.* **18** 7–34
- Hogg E H, Michaelian M, Hook T I and Undershultz M E 2017 Recent climatic drying leads to age-independent growth reductions of white spruce stands in western Canada *Glob. Change Biol.* **23** 5297–309
- Huang K *et al* 2018 Enhanced peak growth of global vegetation and its key mechanisms *Nat. Ecol. Evol.* **2** 1897–905
- Huang K and Xia J 2019 High ecosystem stability of evergreen broadleaf forests under severe droughts *Glob. Change Biol.* **25** 3494–503
- Humphrey V, Zscheischler J, Ciais P, Gudmundsson L, Sitch S and Seneviratne S I 2018 Sensitivity of atmospheric CO<sub>2</sub> growth rate to observed changes in terrestrial water storage *Nature* **560** 628–31
- Ibrahim M A *et al* 2010 Elevation of night-time temperature increases terpenoid emissions from *Betula pendula* and *Populus tremula* *J. Exp. Bot.* **61** 1583–95
- Jing P, Wang D, Zhu C and Chen J 2016 Plant physiological, morphological and yield-related responses to night temperature changes across different species and plant functional types *Frontiers Plant Sci.* **7** 1774
- Joseph T, Whitehead D and Turnbull M H 2014 Soil water availability influences the temperature response of photosynthesis and respiration in a grass and a woody shrub *Funct. Plant Biol.* **41** 468–81
- Karl T R, Kukla G, Razuvayev V N, Changery M J, Quayle R G, Heim R R, Easterling D R and Fu C B 1991 Global warming: evidence for asymmetric diurnal temperature change *Geophys. Res. Lett.* **18** 2253–6
- Klesse S *et al* 2018a A combined tree ring and vegetation model assessment of European forest growth sensitivity to interannual climate variability *Glob. Biogeochem. Cycles* **32** 1226–40
- Klesse S, Deroose R J, Guiterman C H, Lynch A M, O'Connor C D, Shaw J D and Evans M E K 2018b Sampling bias overestimates climate change impacts on forest growth in the southwestern United States *Nat. Commun.* **9** 5336
- Körner C, Asshoff R, Bignucolo O, Hättenschwiler S, Keel S G, Peláez-Riedl S, Pepin S, Siegwolf R T and Zotz G 2005 Carbon flux and growth in mature deciduous forest trees exposed to elevated CO<sub>2</sub> *Science* **309** 1360–2
- Körner C 2003 Carbon limitation in trees *J. Ecol.* **91** 4–17
- Körner C 2013 Growth controls photosynthesis—mostly *Nova Acta Leopoldina NF* **114** 273–83
- Körner C 2015 Paradigm shift in plant growth control *Curr. Opin. Plant Biol.* **25** 107–14
- Liu H *et al* 2013 Rapid warming accelerates tree growth decline in semi-arid forests of Inner Asia *Glob. Change Biol.* **19** 2500–10
- Liu Y Y, Parinussa R M, Dorigo W A, Ram D J, Wagner W, Aijm V D, McCabe M F and Evans J P 2011 Developing an improved soil moisture dataset by blending passive and active microwave satellite-based retrievals *Hydrol. Earth Syst. Sci.* **15** 425–36
- Lloyd A H and Bunn A G 2007 Responses of the circumpolar boreal forest to 20th century climate variability *Environ. Res. Lett.* **2** 045013
- Long S P, Ainsworth E A, Rogers A and Ort D R 2004 Rising atmospheric carbon dioxide: plants FACE the future *Annu. Rev. Plant Biol.* **55** 591–628
- Matsubara S, Hurry V, Druart N, Benedict C, Janzik I, Chavarria-Krauser A, Walter A and Schurr U 2006 Nocturnal changes in leaf growth of *Populus deltoides* are controlled by cytoplasmic growth *Planta* **223** 1315–28
- McDowell N *et al* 2008 Mechanisms of plant survival and mortality during drought: why do some plants survive while others succumb to drought? *New Phytol.* **178** 719–39
- Mkr W, Peláez-Riedl S, Wright S J and Körner C 2004 Non-structural carbohydrate pools in a tropical forest *Oecologia* **143** 11–24
- Muller B, Pantin F, Génard M, Turc O, Freixes S, Piques M and Gibon Y 2011 Water deficits uncouple growth from photosynthesis, increase C content, and modify the relationships between C and growth in sink organs *J. Exp. Bot.* **62** 1715–29
- Myneni R B, Dong J, Tucker C J, Kaufmann R K, Kauppi P E, Liski J., Zhou L, Alexeyev V and Hughes M K 2001 A large carbon sink in the woody biomass of Northern forests *Proc. Natl Acad. Sci. USA* **98** 14784–9
- Nicolai-Shaw N, Zscheischler J, Hirschi M, Gudmundsson L and Seneviratne S I 2017 A drought event composite analysis using satellite remote-sensing based soil moisture *Remote Sens. Environ.* **203** 216–25



- Niu S, Li Z, Xia J, Han Y, Wu M and Wan S 2008 Climatic warming changes plant photosynthesis and its temperature dependence in a temperate steppe of northern China *Environ. Exp. Bot.* **63** 91–101
- Niu S et al 2012 Thermal optimality of net ecosystem exchange of carbon dioxide and underlying mechanisms *New Phytol.* **194** 775–83
- Ogaya R, Peñuelas J, Asensio D and Llusà J 2011 Chlorophyll fluorescence responses to temperature and water availability in two co-dominant Mediterranean shrub and tree species in a long-term field experiment simulating climate change *Environ. Exp. Bot.* **71** 123–7
- Pan Y et al 2011 A large and persistent carbon sink in the world's forests *Science* **333** 988–93
- Papale D, Reichstein M, Aubinet M, Canfora E, Bernhofer C, Kutsch W, Longdoz B, Rambal S, Valentini R and Vesala T 2006 Towards a standardized processing of Net Ecosystem Exchange measured with eddy covariance technique: algorithms and uncertainty estimation *Biogeosci.* **3** 571–83
- Peng S et al 2013 Asymmetric effects of daytime and night-time warming on Northern Hemisphere vegetation *Nature* **501** 88–92
- Peng S, Huang J, Sheehy J E, Laza R C, Visperas R M, Zhong X, Centeno G S, Khush G S and Cassman K G 2004 Rice yields decline with higher night temperature from global warming *Proc. Natl Acad. Sci. USA* **101** 9971–5
- Piao S et al 2014 Evidence for a weakening relationship between interannual temperature variability and northern vegetation activity *Nat. Commun.* **5** 5018
- Pinzon J and Tucker C 2014 A non-stationary 1981–2012 AVHRR NDVI3g time series *Remote Sens.* **6** 6929–60
- Poorter H, Niinemets U, Walter A, Fiorani F and Schurr U 2010 A method to construct dose-response curves for a wide range of environmental factors and plant traits by means of a meta-analysis of phenotypic data *J. Exp. Biol.* **61** 2043–55
- Poorter H, Niklas K J, Reich P B, Oleksyn J, Poot P and Mommer L 2012 Biomass allocation to leaves, stems and roots: meta-analyses of interspecific variation and environmental control *New Phytol.* **193** 30–50
- Reich P B, Sendall K M, Stefanski A, Rich R L, Hobbie S E and Montgomery R A 2018 Effects of climate warming on photosynthesis in boreal tree species depend on soil moisture *Nature* **562** 263–7
- Riahi K, Rao S, Krey V, Cho C, Chirkov V, Fischer G, Kindermann G, Nakicenovic N and Rafaj P 2011 RCP 8.5—a scenario of comparatively high greenhouse gas emissions *Clim. Change* **109** 33–57
- Santoro A E, Lombardero M J, Ayres M P and Ruel J J 2001 Interactions between fire and bark beetles in an old growth pine forest *For. Ecol. Manage.* **144** 245–54
- Schurman J S et al 2019 The climatic drivers of primary Picea forest growth along the Carpathian arc are changing under rising temperatures *Glob. Change Biol.* **25** 3136–50
- Schurr U, Walter A and Rascher U 2006 Functional dynamics of plant growth and photosynthesis—from steady-state to dynamics—from homogeneity to heterogeneity *Plant Cell Environ.* **29** 340–52
- Sheffield J, Goteti G and Wood E F 2006 Development of a 50-year high-resolution global dataset of meteorological forcings for land surface modeling *J. Clim.* **19** 3088–111
- Steppe K, Sterck F and Deslauriers A 2015 Diel growth dynamics in tree stems: linking anatomy and ecophysiology *Trends Plant Sci.* **20** 335–43
- Tan J et al 2015 Seasonally different response of photosynthetic activity to daytime and night-time warming in the Northern Hemisphere *Glob. Change Biol.* **21** 377–87
- Tei S, Sugimoto A, Kotani A, Ohta T, Morozumi T, Saito S, Hashiguchi S and Maximov T 2019 Strong and stable relationships between tree-ring parameters and forest-level carbon fluxes in a Siberian larch forest *Polar Sci.* **21** 146–57
- Tei S, Sugimoto A, Yonenobu H, Matsuura Y, Osawa A, Sato H, Fujinuma J and Maximov T 2017 Tree-ring analysis and modeling approaches yield contrary response of circumboreal forest productivity to climate change *Glob. Change Biol.* **23** 5179–88
- Teuling A J et al 2010 Contrasting response of European forest and grassland energy exchange to heatwaves *Nat. Geosci.* **3** 722–7
- Thomson A M et al 2011 RCP4.5: a pathway for stabilization of radiative forcing by 2100 *Clim. Change* **109** 77–94
- Turnbull M H, Murthy R and Griffin K L 2002 The relative impacts of daytime and night-time warming on photosynthetic capacity in *Populus deltoides* *Plant Cell Environ.* **25** 1729–37
- Turnbull M H, Tissue D T, Murthy R, Wang X, Sparrow A D and Griffin K L 2004 Nocturnal warming increases photosynthesis at elevated CO<sub>2</sub> partial pressure in *Populus deltoides* *New Phytol.* **161** 819–26
- Vaganov E A, Hughes M K and Shashkin A V 2006 *Growth Dynamics of Conifer Tree Rings: Images of Past and Future Environments* (Berlin: Springer)
- van Mantgem P J, Nesmith J C, Keifer M, Knapp E E, Flint A and Flint L 2013 Climatic stress increases forest fire severity across the western United States *Ecol. Lett.* **16** 1151–6
- Vicente-Serrano S M et al 2013 Response of vegetation to drought time-scales across global land biomes *Proc. Natl Acad. Sci. USA* **110** 52–57
- Walter A, Christ M M, Barron-gafford G A, Grieve K A, Murthy R and Rascher U 2005 The effect of elevated CO<sub>2</sub> on diel leaf growth cycle, leaf carbohydrate content and canopy growth performance of *Populus deltoides* *Glob. Change Biol.* **11** 1207–19
- Wan S, Xia J, Liu W and Niu S 2009 Photosynthetic overcompensation under nocturnal warming enhances grassland carbon sequestration *Ecology* **90** 2700–10
- Way D A and Oren R 2010 Differential responses to changes in growth temperature between trees from different functional groups and biomes: a review and synthesis of data *Tree Physiol.* **30** 669–88
- Williams A P, Allen C D, Millar C I, Swetnam T W, Michaelsen J, Still C J and Leavitt S W 2010 Forest responses to increasing aridity and warmth in the southwestern United States *Proc. Natl Acad. Sci. USA* **107** 21289–94
- Williams A P et al 2012 Temperature as a potent driver of regional forest drought stress and tree mortality *Nat. Clim. Change* **3** 292–7
- Wilson R J S and Luckman B H 2002 Tree-ring reconstruction of maximum and minimum temperatures and the diurnal temperature range in British Columbia, Canada *Dendrochronologia* **20** 257–68
- Xia J, Chen J, Piao S, Ciais P, Luo Y and Wan S 2014 Terrestrial carbon cycle affected by non-uniform climate warming *Nat. Geosci.* **7** 173–80
- Yuan W et al 2011 Thermal adaptation of net ecosystem exchange *Biogeosci.* **8** 1453–63